Probing the integrin-actin linkage using high-resolution protein velocity mapping

Claire M. Brown[1,*,‡], Benedict Hebert[2], David L. Kolin[3], Jessica Zareno[1], Leanna Whitmore[1], Alan Rick Horwitz[1] and Paul W. Wiseman[2,3]

[1]Department of Cell Biology, University of Virginia, Charlottesville, VA, USA
[2]Department of Physics, [3]Department of Chemistry, McGill University, Montreal, Canada

*Author for correspondence (e-mail: claire.brown@mcgill.ca)
‡Present address: Life Sciences Complex Imaging Facility, Department of Biochemistry, McGill University, Montreal, Canada

Accepted 30 October 2006
Journal of Cell Science 119, 5204-5214 Published by The Company of Biologists 2006
doi:10.1242/jcs.03321

Summary

Cell migration is regulated in part by the connection between the substratum and the actin cytoskeleton. However, the very large number of proteins involved in this linkage and their complex network of interactions make it difficult to assess their role in cell migration. We apply a novel image analysis tool, spatio-temporal image correlation spectroscopy (STICS), to quantify the directed movements of adhesion-related proteins and actin in protrusions of migrating cells. The STICS technique reveals protein dynamics even when protein densities are very low or very high, and works in the presence of large, static molecular complexes. Detailed protein velocity maps for actin and the adhesion-related proteins α-actinin, α5-integrin, talin, paxillin, vinculin and focal adhesion kinase are presented. The data show that there are differences in the efficiency of the linkage between integrin and actin among different cell types and on the same cell type grown on different substrate densities. We identify potential mechanisms that regulate efficiency of the linkage, or clutch, and identify two likely points of disconnect, one at the integrin and the other at α-actinin or actin. The data suggests that the efficiency of the linkage increases as actin and adhesions become more organized showing the importance of factors that regulate the efficiency in adhesion signaling and dynamics.

Supplementary material available online at
http://jcs.biologists.org/cgi/content/full/119/24/5204/DC1

Key words: Adhesion, Cell migration, Actin, Adhesion-associated proteins, Image correlation spectroscopy, Velocity mapping

Introduction

Cell migration results from the integration of several component processes including the formation and stabilization of protrusions, and the assembly and disassembly of adhesions (Lauffenburger and Horwitz, 1996; Ridley et al., 2003). Whereas protrusions are generated by actin polymerization, the protrusion rate can be modulated by the relative rate of retrograde actin flow, which is adhesion dependent (Mitchison and Kirschner, 1988; Peskin et al., 1993). The assembly of adhesions is regulated, in part, by the tension sensed by adhesions, which serve as both signaling centers and traction points for the generation of tension (Crowley and Horwitz, 1995; Ridley et al., 2003). Therefore, adhesion and protrusion are interconnected and can be controlled by the efficiency of the linkage between the extra-cellular matrix (ECM) and actin. Thus, this linkage emerges as a potential regulatory mechanism for protrusion and migration.

Despite its importance, few studies have addressed the ECM-actin linkage and its regulation in migrating cells. The role of integrins in the linkage has been studied in retracting regions at the rear of migrating cells (Palecek et al., 1998; Palecek et al., 1996; Regen and Horwitz, 1992). In these regions, the linkage severs between integrin and other adhesion components leaving integrin-containing 'footprints' on the substratum, often with an accompanying sliding of the remaining adhesion toward the cell cortex (Palecek et al., 1996; Regen and Horwitz, 1992; Smilenov et al., 1999). The amount of integrin in the footprints depends on parameters that contribute to adhesion strength such as the concentration of ECM proteins, the number of integrin receptors, the affinity of integrin for the ECM, as well as calpain activity (Palecek et al., 1998). These observations suggest that, for retracting regions of the cell, the bond between the ECM and integrin is much stronger than that linking integrin to the cytoskeleton (Palecek et al., 1998; Palecek et al., 1996; Regen and Horwitz, 1992). Recently, paxillin was observed in the footprints of focal adhesion kinase (FAK)-null cells, suggesting that FAK regulates a labile site in the linkage (Webb et al., 2004). These observations lead to a hypothesis in which the linkage between the ECM and actin is regulated by changes in interactions among linkage components through the action or modification by signaling molecules such as Src, paxillin and FAK. The challenge, therefore, is to define the nature and regulation of the linkage in migrating cells.

A plethora of in vitro studies point to interactions among integrin, talin, vinculin, α-actinin and actin as likely crucial elements of the linkage from the ECM to actin (Burridge and Mangeat, 1984; Burridge et al., 1990; Horwitz et al., 1986; Otey et al., 1990; Pavalko and Burridge, 1991; Sato et al., 1987). Adhesion-associated signaling components, such as

FAK, Src and paxillin, could then regulate the ECM-actin linkage through modifications that result in altered affinities, e.g. phosphorylation or enzymatic cleavage, of proteins that comprise the linkage. Such studies would benefit greatly from quantitative estimates of the efficiency of the linkage in situ and the roles of various adhesion components in determining its efficiency. However, it is difficult to clearly define and characterize the molecular basis of the ECM-integrin-actin linkage in living cells because of the complex interactions in space and time between integrins and adhesion proteins (Vicente-Manzanares et al., 2005) and the diverse kinetic and kinematic behaviors of the cytoskeleton (Ponti et al., 2004).

Recently, there have been significant advances in cellular imaging tools and techniques that allow this problem to be approached via direct measurements inside cells. In situ experiments using chromophore-assisted laser inactivation (CALI) have implicated talin as a crucial molecule in the ECM-actin linkage during filopodial extension and retraction (Sydor et al., 1996). More recently, extensive characterization of actin dynamics using fluorescent speckle microscopy (FSM) (Waterman-Storer et al., 1998) has revealed two spatially, kinetically and kinematically distinct actin networks; with the local expansion of the lamella network being a source of persistent cell protrusion (Ponti et al., 2004). There is also evidence that the actin network is dynamically coupled to adhesions (Jurado et al., 2005; Vallotton et al., 2005) by a biphasic relationship between the retrograde flow of actin and the cell-substratum adhesiveness (Gupton and Waterman-Storer, 2006; Jurado et al., 2005). Nevertheless, to date, the dynamics of the integrin linkage to actin has not been systematically studied during migration.

Here, we describe a general velocity-mapping technique termed spatio-temporal image correlation spectroscopy (STICS) that is based on the analysis of sequences of fluorescence microscope images (Hebert et al., 2005). We validate the technique by quantifying actin and α-actinin flow and comparing them to the known retrograde dynamics of actin flow. We then apply STICS to generate co-transport maps of actin and a set of adhesion and actin-binding proteins near the basal membrane in protrusions in doubly transfected Chinese hamster ovary (CHO) cells or mouse fibroblast (MEF or 3T3) cells. The detailed cellular maps of molecular transport that we generate allow us to quantify coupling between adhesion components and actin, identify some parameters that influence it and thus provide new insight into the mechanistic details of the ECM-integrin-actin protein linkage in different cell types during cell protrusion and migration.

Results

STICS

The STICS technique detects directed movements of macromolecules (e.g. fluorescent proteins) from the analysis of fluorescence image time series. The technique can even detect motion in regions in which the fluorescence appears to the eye to be homogeneous (as long as protein densities are not too high, see Materials and Methods). STICS can also detect components undergoing directed movement when they represent as little as 10% of the total population, or within bright immobile structures such as adhesions or actin filaments.

The technique involves calculating the spatial-temporal correlation function as a function of time lag between all possible sets of image pairs within an image time series. If proteins are simply diffusing, then the central peak of the spatial-temporal correlation function will remain centered and decay in amplitude, and broaden as the time lag between image pairs is increased (Fig. 1D). However, if there is a persistent directed motion of macromolecules there will be an additional correlation flow-component peak that begins at the origin (at zero time lag) and moves in the direction opposite to that of the macromolecule flow (Fig. 1B, arrowhead) but at the same rate as the molecular speed. Tracking of this peak over time reveals protein velocity.

Cells frequently have relatively immobile macroscopic, multi-component complexes, such as adhesions or cytoskeletal filaments and associated proteins. These relatively static structures dominate the spatial correlation function, and the flow component correlation peak is 'buried' by the persistence of the central static correlation peak (Fig. 1B, arrowhead). An immobile removal algorithm was developed to reveal only the flow-component peak in the correlation function (Fig. 1C, for details see Materials and Methods). Computer simulations demonstrate that the algorithm efficiently removes the contributions of any static components and measures velocities accurately (see Materials and Methods). Note that, if some components are undergoing transient binding and unbinding to adhesions or filaments, they will not be removed by the filtering algorithm because they are not immobile over the entire time course of the measurement. STICS can accurately measure velocities when the immobile 'background' contributes up to 90% of the total intensity. Therefore, even in the presence of large static structures within the cell, such as adhesions or actin filaments, the STICS analysis, combined with the immobile filtering algorithm, allows us to map the dynamics of any proteins moving within or along these structures.

Validation of STICS technique

To validate the STICS technique for our application, MEF cells were transfected with α-actinin-EGFP and mRFP-actin and imaged using total internal reflection fluorescence (TIRF) microscopy, which selectively images near the basal surface of the cell because only fluorescent molecules within 50-100 nm of the coverslip are excited (Axelrod, 2001). The analysis was performed on small (2-3 μm square boxes) overlapping sub-regions within the original image time series to generate detailed protein velocity maps of the cell (Fig. 2A). Two simultaneous velocity maps were generated to compare the co-transport of α-actinin with actin. Owing to the dependence of the retrograde velocities on the protrusion rate, substrate adhesiveness and the rate of actin polymerization, which varies between cells (Lin and Forscher, 1995) and between different regions of the same cell, the absolute values of the protein velocities were not directly compared. Instead velocities relative to the velocity of actin within each sub-region were used as a measure of the degree of interaction between actin and the adhesion proteins. To quantify these interactions, two scores were calculated: the first is a correlation coefficient between the magnitudes of the velocities, the second a correlation coefficient between the directions of the velocity vectors. The directional correlation score varies between –1 and 1; a score of 1 being perfectly aligned velocity maps, zero being totally uncorrelated flow fields and –1 being velocities in opposite directions (see Materials and Methods).

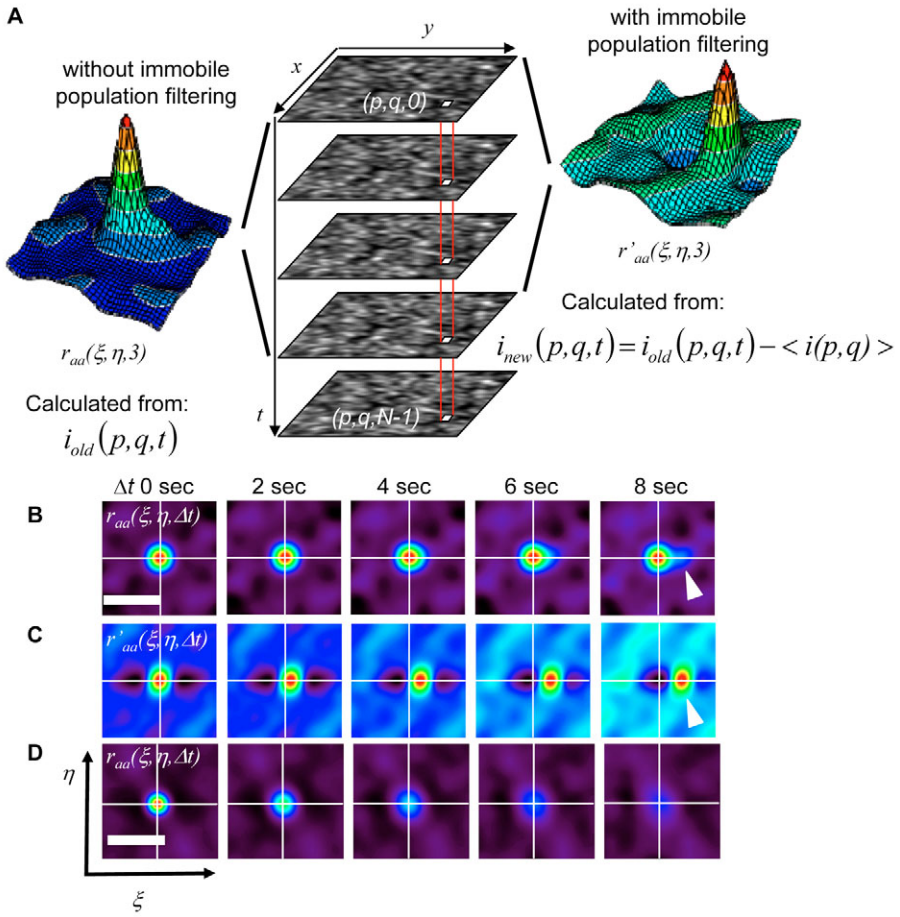

Fig. 1. (A) Analysis of a computer-simulated image time series of a flowing particle population (20% of the total particle density, v_x=–0.1 μm/second, v_y=0 μm/second) superimposed over an immobile particle population (80% of the total particle density). The average spatial correlation function for a lag time Δt=3 seconds is calculated from the original intensities [$r_{aa}(\xi,\eta,3)$, left] and from the immobile filtered intensities [$r'_{aa}(\xi,\eta,3)$, right]; note the small flow component correlation peak that appears on the left side of the central correlation function without immobile filtering, this flow component peak is all that is seen in the function after immobile filtering. Contour plots of STICS correlation functions $r_{aa}(\xi,\eta,\Delta t)$ as a function of lag time for the simulation above without (B) and with (C) immobile population filtering. Contour plots for a simulation of particles undergoing pure diffusion at 0.01 μm^2/second (D). Bar, 2 μm.

The immobile removal algorithm allowed us to follow the flow-component peak buried under the central correlation peak arising from the dominant static spatial correlations of the bright filamentous structures within the images (Fig. 2, compare B and C, arrowhead identifies the flow-component peak) and to map the movement of α-actinin and actin along the filaments (Fig. 2A, supplementary material Movie 1AB). The velocity rates ranged from ~0.02 μm/minute (blue arrows) to 0.3 μm/minute (red arrows), comparable with those previously measured for actin using fluorescence speckle microscopy (FSM) (Ponti et al., 2004; Vallotton et al., 2003). Note the heterogeneity in the velocity magnitudes, which are represented by the different colored vectors, across the lamellum. Also note that, in regions at the rear of the lamellum near the nucleus, the rate of flow is greatly diminished, i.e. <0.1 μm/minute (Fig. 2A, predominantly blue vectors in the upper middle part of the images), relative to regions near the leading edge of the protrusion. The flow fields were compared, and the median velocity magnitude for α-actinin relative to actin was 0.83±0.03 and the median directional correlation was 0.92±0.01, demonstrating that the movement of α-actinin is highly correlated with the movement of actin in situ.

To further confirm the validity of the STICS technique, we compared velocities determined by FSM analysis to those determined by STICS. The Quicktime movie from fig. 1A of Ponti et al. (Ponti et al., 2004) was analysed by STICS. The velocity field derived by their FSM tracking analysis was very similar to that derived by STICS; compare Fig. 3 in this article with fig. 1A in Ponti et al. (Ponti et al., 2004).

Both actin polymerization and myosin-II-mediated contraction are reported to inhibit retrograde flow (Ponti et al., 2004; Jurado et al., 2005). Cells were imaged for 10-20 minutes before and after treatments with inhibitors. The measurements before and after treatment were compared in two ways: (1) changes in the velocity and directional correlation of α-actinin relative to actin and, (2) changes in the velocity and directional movements of each protein, α-actinin or actin, relative to itself. Cytochalasin D (cytoD), stops protrusion by inhibiting the polymerization of actin-free barbed ends (Sampath and Pollard, 1991). The velocity maps of α-actinin and actin computed before and after addition of drug revealed that both the actin and the α-actinin velocities were reduced to about half of their pre-treatment velocities

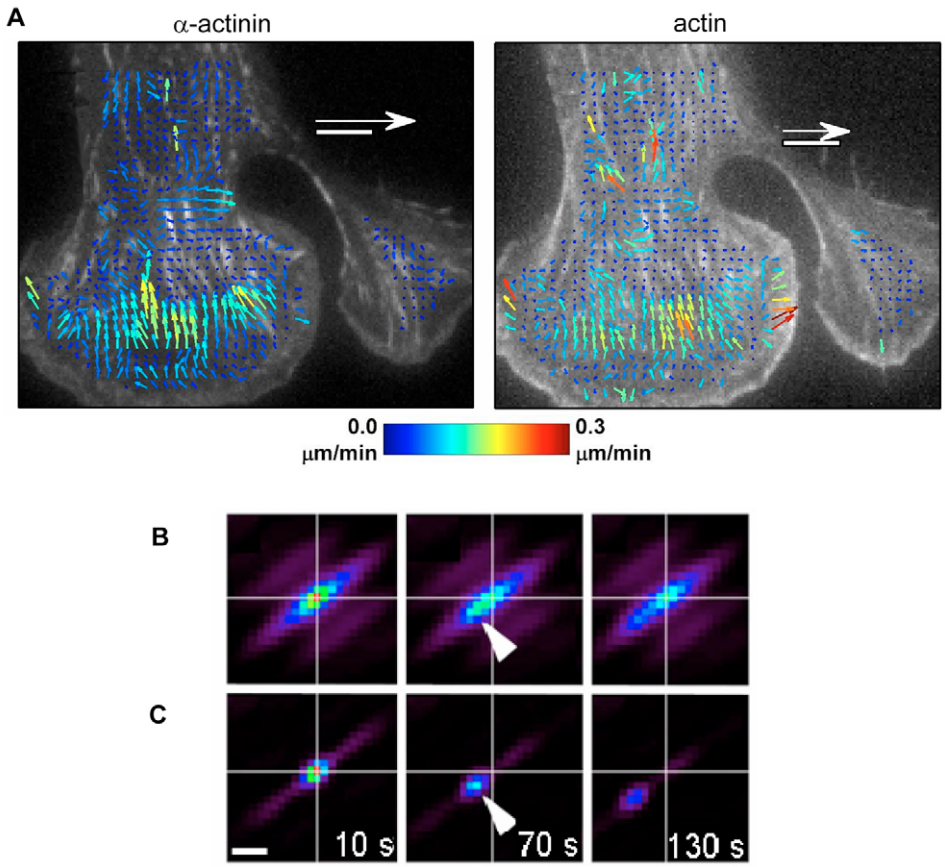

Fig. 2. (A) Velocity maps of α-actinin-EGFP and mRFP-actin in a MEF cell plated on 1 μg/ml fibronectin. Analysis was performed on 100 frames imaged at 10 seconds per frame. The color-coding for the velocity vectors is universal within the figure with blue being slow velocities and red being faster velocities. The scale of the velocity vectors is different for each plot and is referenced on each image with a 0.5 μm/minute velocity scale arrow. Spatial scale bar is 5 μm. Pixel size is 0.215 μm. (B) Sample STICS correlation function showing that flow-component peak tracking is quite difficult without immobile population filtering (arrowhead). (C) After immobile population removal, a clear displacement of the flow component peak can be observed (white arrowhead) and tracked to reveal the direction and magnitude of the velocity. This filtering removes the contribution to the correlation function of the large static features, i.e. the actin filament structures. Bar, 1 μm.

following treatment with 200 nM cytoD (actin 55±7%, α-actinin 53±6%, Fig. 4A,B). The relative flow direction before and after cytoD treatment for both α-actinin (Fig. 4B) and actin (data not shown) completely changed so that on average the motions were unrelated to their original trajectories (Fig. 4B). Although the median velocities and directions of movement for both α-actinin and actin changed following cytoD treatment, the two proteins remained coupled, because their relative magnitude (0.71±0.13 before and 0.77±0.05 after treatment) and directional correlation coefficients (0.78±0.02 before and 0.83±0.06 after treatment) were not affected.

To examine the role of myosin-II-mediated contraction in the retrograde protein flow, three inhibitors were used. The ATPase activity of non-muscle myosin II was inhibited with 50 μM blebbistatin (Straight et al., 2003), and myosin-II-activation was inhibited using either the ROCK inhibitor Y-27632 (10 μM) or the MLCK inhibitor ML7 (10 μM). Similar to cytoD treatment, all three inhibitors reduced the velocity of α-actinin (relative magnitude, Fig. 4B) and actin (data not shown) flow to ~60% of pre-treatment velocities. However, α-actinin and actin remained coupled following the treatments, i.e. the relative velocities and relative directions of the flow vectors before and after treatment were similar (data not shown). As with the cytoD treatment, each of the other three treatments produces a major change in the direction of movement of both α-actinin (directional correlation, Fig. 4B) and actin (data not shown). In some of the sub-regions the proteins reverse direction, giving rise to a negative directional correlation, i.e. anteretrograde flow (Fig. 4B). Taken together, these measurements are similar to those seen using FSM (Ponti et al., 2004; Jurado et al., 2005) and thus validate and establish the generality of the STICS method for producing high-resolution velocity maps in situ.

The integrin-actin linkage in CHO cells

The linkage between integrin and actin was first investigated in highly dynamic CHO cells. The cells were plated for 30-60 minutes at 37°C under migration-promoting conditions on coverslips that were coated with a low concentration of fibronectin (2 μg/ml). Under these conditions CHO cells protrude rapidly (0.7-6 μm/minute), have relatively small adhesions (Fig. 5A, e.g. integrin and paxillin), and do not contain highly organized actin stress fibers (Fig. 5A) (Laukaitis et al., 2001). CHO cells plated under these conditions do not

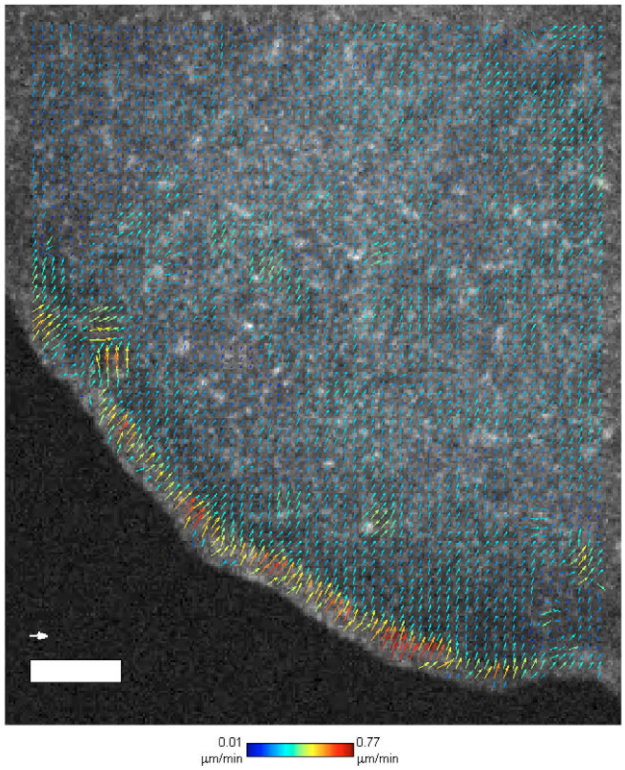

Fig. 3. STICS analysis of a Quicktime movie from fig. 1A described in Ponti et al. (Ponti et al., 2004). Scale bar, 5 μm; velocity scale bar, 0.5 μm/minute. The data matches very well with data calculated using speckle tracking in the paper, revealing faster dynamics within the lamellipodia at the edge of the cell and slower dynamics in the lamella. Note that the analysis was done on the Quicktime movie and some data compression may have occurred relative to the raw speckle data. Also, the pixel size was estimated using the scale bar from the figure so velocity estimates are only approximate.

show large organized adhesions in active protrusions, or prominent actin stress fibers. However, we have previously shown that, even under these conditions, the integrin is clustered and organized in immobile structures that are not visible by eye (Wiseman et al., 2004).

A series of EGFP-fusion proteins, including α5-integrin, paxillin, FAK, talin, vinculin and α-actinin, were co-expressed transiently with mRFP-actin. Like in MEF cells (Fig. 2A), α-actinin and actin in CHO cells have very similar flow fields with a directional correlation of 0.64±0.15 and a relative magnitude correlation of 0.81±0.28 (Fig. 5A,B). However, the flow fields are not as uniform or homogeneous as those seen in the more adherent MEF cells (compare Fig. 2A and Fig. 5A). By contrast, other adhesion-associated proteins, e.g. paxillin (supplementary material Movie 3AB), FAK, talin (supplementary material Movie 3CD) and vinculin, have a low directional correlation with actin (<0.3; Fig. 5A,B), and their velocity magnitudes are significantly smaller (Fig. 5A,B). In addition, the velocity vectors (Fig. 5A) do not show a uniform field of retrograde protein movement like that seen for α-actinin and actin in the MEF cells (Fig. 2A). This difference probably reflects the differences in organization of the actin and adhesions in the two different cell types. Integrin velocities were slow throughout the lamella (magnitude correlation; 0.37±0.16) and also showed little directional correlation (0.11±0.15) with the actin flow (Fig. 5A,B). Temporal image correlation spectroscopy analysis shows that >80% of the integrins are stationary relative to the substrate (Table 1), in accord with our earlier image correlation and FRAP measurements (Wiseman et al., 2004).

Taken together, the data support the notion of a strong interaction between α5-integrin and the ECM, and a weaker interaction between actin and the adhesion-associated proteins in active protrusions in CHO cells. The dynamics of the adhesion-associated proteins are similar to the dynamics of integrin (Fig. 5B), and we find that a large percentage of the adhesion proteins are also immobile (60-70%; Table 1), suggesting that these proteins are more tightly associated with integrin than actin (Table 1). Note that the STICS analysis only measures the directed movement of proteins that are mobile on the time scale of the experiments (5-20 minutes).

The integrin-actin linkage in mouse fibroblasts

Since the coupling between adhesion-associated proteins and actin was weak in CHO cells, we investigated mouse fibroblasts (3T3 and MEF), which have more highly organized actin filaments and larger adhesions (compare Fig. 5A with Fig. 6A). As presented above, α-actinin and actin have very uniform flow fields, and their flow is tightly coupled in MEF cells (Fig. 2A), with a directional correlation of 0.87±0.10 and a relative velocity magnitude of 0.75±0.13. By contrast, the integrin is essentially immobile (Table 1), with less than 10% moving, and the direction that it moves is not highly correlated with actin movement (directional correlation of 0.19±0.34). STICS analysis also revealed much more uniform, homogenous flow fields for paxillin (supplementary material Movie 4AB), FAK, talin and actin, when compared with the CHO cells (Fig. 6A). In further contrast to CHO cells, all three adhesion-associated proteins showed high directional correlations with actin (Fig. 6B, gray bars), and the velocity magnitudes of these proteins were ~65-70% of the magnitude of actin (Fig. 6A,B, black bars). When the directional correlations are high, a relative velocity magnitude less than one suggests that the adhesion-associated proteins are immobilized when they are not bound to actin and are undergoing a transient binding and unbinding. That is, when the proteins are bound to actin (70% of the measurement time) they are moving at the same speed as actin, but when not bound to actin (30% of the measurement time) they are immobile. This would result in an apparent velocity magnitude that is 30% lower than that of actin. Note that, the velocity vectors shown are displayed in the center of the analysis region, which extends ~1 μm from the vectors in all directions (see FAK panel Fig. 6A). However, the vectors are not calculated right up to the edge of the cell because edges can create artifacts in the analysis.

To verify that the measurements in 3T3 cells were dominated by the dynamics of proteins within adhesions, image time series of cells expressing talin-EGFP within long adhesions were examined. The longer adhesions on these cells allowed sufficient sampling for the STICS analysis to be performed on a rectangular sub-region encompassing only the adhesion. Vector mapping along the adhesion (supplementary material Fig. S1B, white rectangle and arrow) repeatedly gives essentially the same velocity vector as analysis within the standard 16×16 pixel

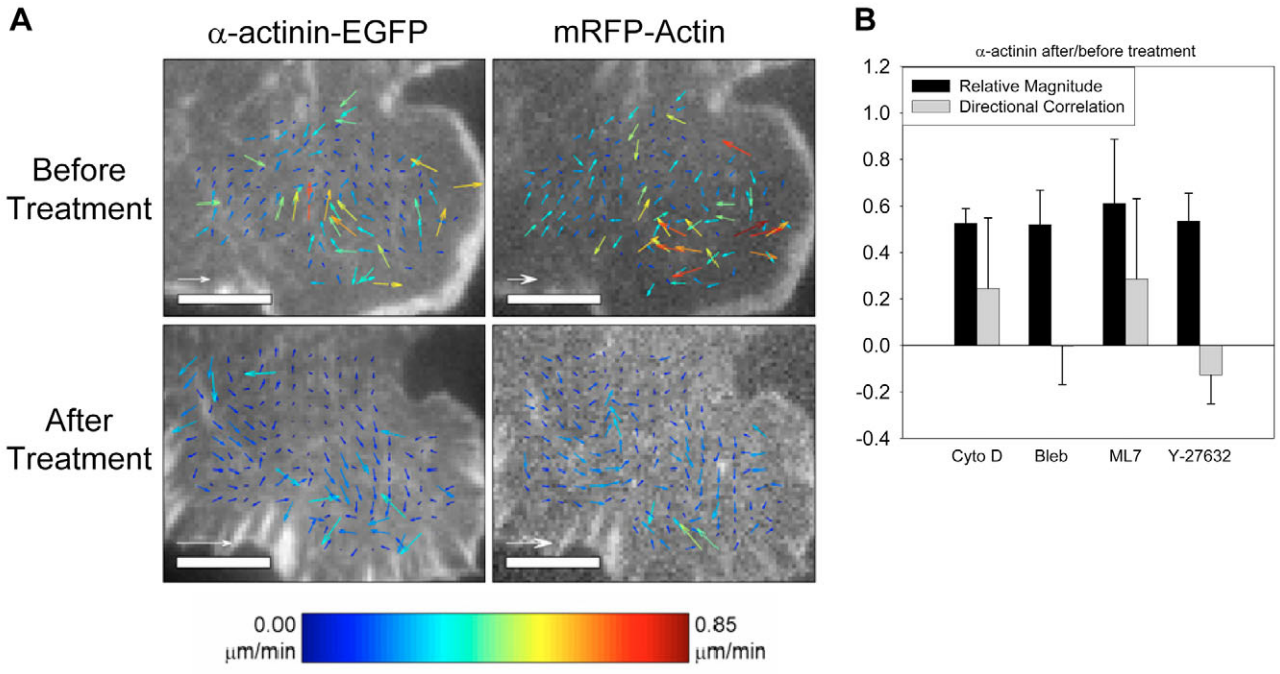

Fig. 4. (A) Velocity maps of α-actinin and actin in a CHO cell plated on 2 μg/ml fibronectin before and after treatment with cytochalasin D (200 nM). The image time series were 200 frames at a rate of 5 seconds/frame. The analysis was done on 100 image frames before and after treatment. The color-coding for the velocity vectors is universal within the figure with blue being slow velocities and red being faster velocities. The scale of the velocity vectors is different for each plot and is referenced on each image with a 0.5 μm/minute velocity scale arrow. Spatial scale bar is 5 μm. (B) Median relative magnitude (black bars) and directional (gray bars) coefficients of velocity vectors after treatment relative to those before for α-actinin with inhibitors. A value of 1.0 represents no change. Results were similar for actin. Error bars give the s.d.

square region encompassing the adhesion and some surrounding area (supplementary material Fig. S1B, red square and arrow). Furthermore, no flow was detected in a velocity map of a sub-region that did not overlap with visible adhesions (supplementary material Fig. S1B, white square with X). Thus, the analyses on the fibroblasts are dominated by movements within or along the prominent, highly organized adhesions.

CHO cells on high concentrations of fibronectin

The differences between CHO cells and mouse fibroblasts could arise from intrinsic differences in cell types or from the differences in organization of actin and adhesions. To test this, we increased the fibronectin concentration on which the CHO cells were plated (from 2 μg/ml to 5 μg/ml). CHO cells plated on higher concentrations of fibronectin have larger more highly organized adhesions, and more organized actin stress fibers (Fig. 7A, supplementary material Movie 5AB). The cells move more slowly (Laukaitis et al., 2001), fewer cells protrude and of those that do protrude the protrusion rates are slower (1.5±0.8 on 5 μg/ml fibronectin versus 2.7±1.6 on 2 μg/ml fibronectin; $P<0.005$). The STICS analysis show that, on higher fibronectin there was a marked increase in the directional correlation for both talin (from 0.01±0.15 on 2 μg/ml fibronectin to 0.32±0.12; $P<0.004$) and paxillin (from 0.15±0.22 on 2 μg/ml fibronectin to 0.52±0.23, $P<0.004$) relative to actin (Fig. 7A,B). Interestingly, in retracting regions of CHO cells plated on low fibronectin concentration (2 μg/ml), where actin and adhesions are also more organized, the correlation between talin and actin also increases significantly (directional correlation =0.8; supplementary material Fig. S2; Movie AB). These data suggest that the strength of the integrin-actin linkage is coupled to actin and adhesion organization.

Discussion

Regulation of the linkage between the ECM and the actin cytoskeleton is crucial for cell migration. The linkage is important for regulating protrusion formation, the rate of protrusion, protrusion stability and the rate of retraction. In addition, the linkage contributes to adhesion assembly, turnover and signaling by coupling myosin mediated contraction forces to the adhesions (Dobereiner et al., 2005; Geiger and Bershadsky, 2001; Geiger and Bershadsky, 2002; Geiger et al., 2001; Katsumi et al., 2005). In this study we have addressed the efficiency of the ECM-actin linkage and its regulation. We have done this by adapting and applying a new image correlation method, STICS, which allows the generation of high-resolution velocity maps of fluorescent protein dynamics throughout the cell. Flow velocities for a number of adhesion components, e.g. α5-integrin, α-actinin, paxillin, FAX, talin and vinculin, were compared with those of actin to determine the efficiency of the integrin-actin linkage and to identify which proteins within the linkage are potential sites of regulation via transient decoupling or slippage.

Previous studies have pointed to integrins as the link between the ECM and actin, making the binding between integrin or actin with cytoplasmic adhesion components potential sites of decoupling (Palecek et al., 1998; Palecek et al., 1996; Smilenov et al., 1999). At the cell rear, the strength of integrin binding to the substratum depends on the affinity of

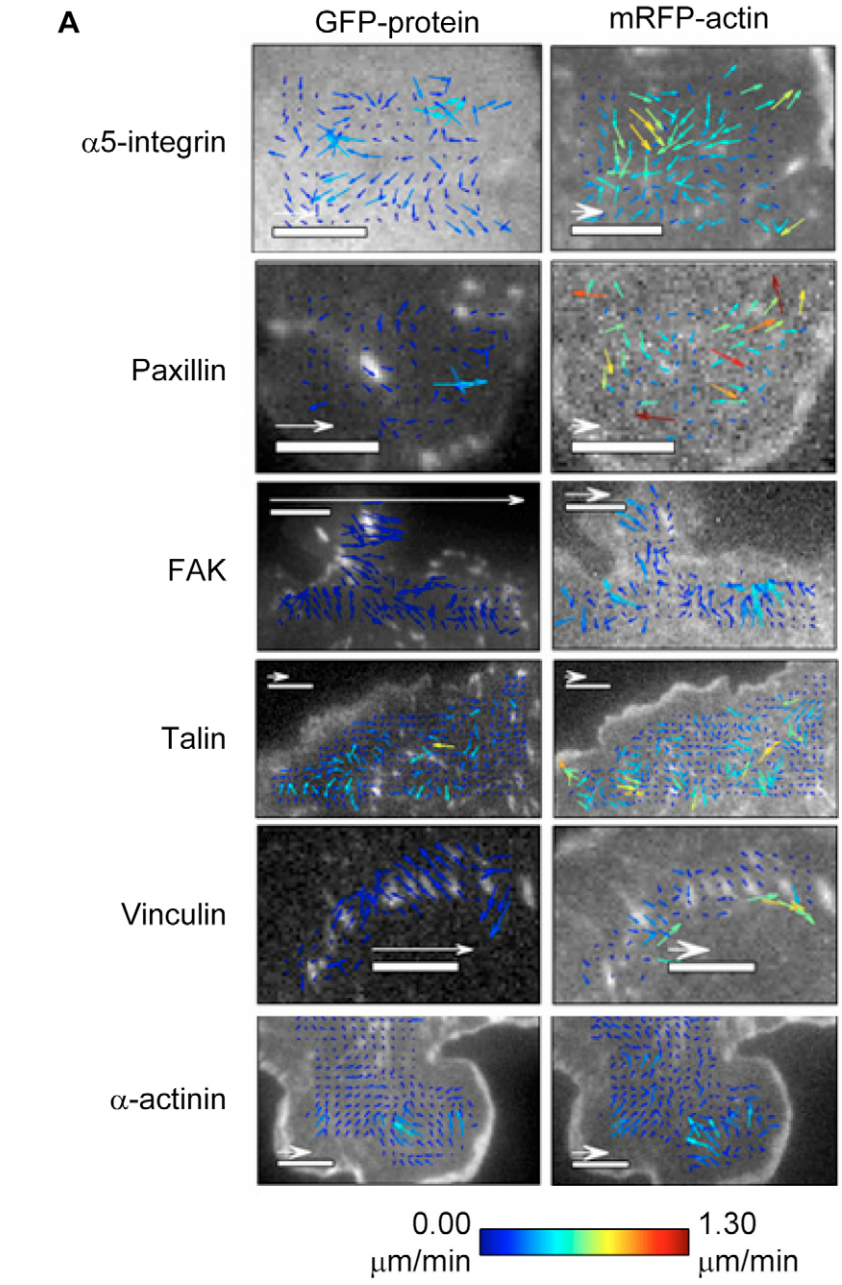

Fig. 5. Protein velocity maps for CHO K1 cells co-transfected with an adhesion protein-EGFP and actin-mRFP and plated on 2 μg/ml fibronectin. (A) Velocity maps in protruding regions of the cell for EGFP conjugated with α5-integrin (96 frames analysed), paxillin (51 frames analysed), FAK (50 frames analysed), talin (55 frames analysed), vinculin (30 frames analysed), α-actinin (100 frames analysed) and the corresponding actin-mRFP velocity maps. The color coding for the velocity vectors is universal with blue being slow velocities and red being faster velocities. The scale of the velocity vectors is different for each plot and is referenced on each image with a 0.5 μm/minute velocity scale arrow. Spatial scale bars are 5 μm. (B) Plot of the median relative magnitude and directional correlation coefficient scores relative to actin for each protein in CHO cells. Pixel size of 0.215 μm. Error bars give the s.d.

the integrin to the ECM, the concentration of fibronectin on the substratum, and the number of integrin receptors (Palecek et al., 1998; Palecek et al., 1996; Smilenov et al., 1999). The studies presented here show that the binding of integrin to the substratum is also strong in the lamella of migrating cells where upwards of 80% of the integrin is immobile.

Under migration-promoting conditions, e.g. cells plated for short times (<3 hours) on low fibronectin concentration (2 μg/ml), CHO cells do not form highly organized stress fibers or many large adhesions, and they protrude and retract frequently. This is typical of many highly motile cells and suggests that high motility is mediated by small dynamic adhesions that are not connected to the highly organized actin filament bundles that are readily visualized in the light microscope. Under these conditions, the STICS analysis shows that, whereas α-actinin and actin are highly coupled in their movements, the movements of paxillin, FAK, talin and vinculin are not tightly coupled to actin movement. The disconnect between actin and integrin in the protrusions of CHO cells suggests that there is less tension on the adhesions and, thus, actin filaments are less well organized and adhesions are smaller. Mouse fibroblasts (MEF or 3T3 cells), which have more highly organized actin filaments and larger adhesions, show more tightly coupled dynamics between actin and adhesion components like paxillin, FAK, and talin. This suggests that there is a much tighter coupling between adhesions and actin in these cells. This effect of the strength of adhesion on coupling and actin organization is supported by observations that the coupling between talin or paxillin and actin is enhanced when CHO cells are plated on a high concentration of fibronectin (5-10 μg/ml). These cells also show larger adhesions, more organized actin, and a tighter dynamic coupling between adhesion

Table 1. Temporal image correlation analysis

Protein	Immobile proteins (%)
Integrin	88*±5
Paxillin	74±14
FAK	74±15
Talin	63±16
Vinculin	66±20
α-actinin	56±21
Actin	28±9

The percentage of immobile proteins was calculated based on the amplitude of the temporal auto-correlation function and the amplitude of the auto-correlation-function offset due to the immobile component (Wiseman and Brown et al., 2004). All measurements were taken in regions of the cell that showed visible adhesions except for integrin measurements (because adhesions were not visible).

*For immobile fractions >90% it is difficult to fit the temporal correlation function because it does not decay very much. When the functions could not be fit, an immobile fraction of 90% (rather than 100%) was assumed, although in some cases the fraction might be even higher. Thus, 88% is the minimum percentage of immobile integrin. Errors are s.d.

components and actin. Thus, it appears that the efficiency of the linkage between integrin and actin is regulated by the adhesion strength. This leads to a model in which increased adhesion strength promotes increased coupling between adhesions and actin; the more efficient linkage, in turn, serves to increase the tension on adhesions and promote their maturation as well as actin bundling. Thus the efficiency of the linkage or clutch becomes a mechanism for regulating adhesion signaling, maturation and dynamics.

The very similar level of coupling to actin shown by paxillin, FAK and talin in 3T3 cells suggests that all three proteins reside in a common complex that is linked to integrin and actin through common mechanisms. In CHO cells, the adhesion proteins are not highly directionally coupled to actin and appear to be primarily associated with immobile integrin (Fig. 8A). By contrast, in mouse fibroblasts these proteins show velocity magnitudes that are 70% of that of actin, suggesting that the linkage complex is bound to actin 70% of the time (Fig. 8B) and to immobilized integrin 30% of the time (Fig. 8A).

Taken together, the data suggest that the linkage between the ECM and actin is regulated by adhesion strength. This

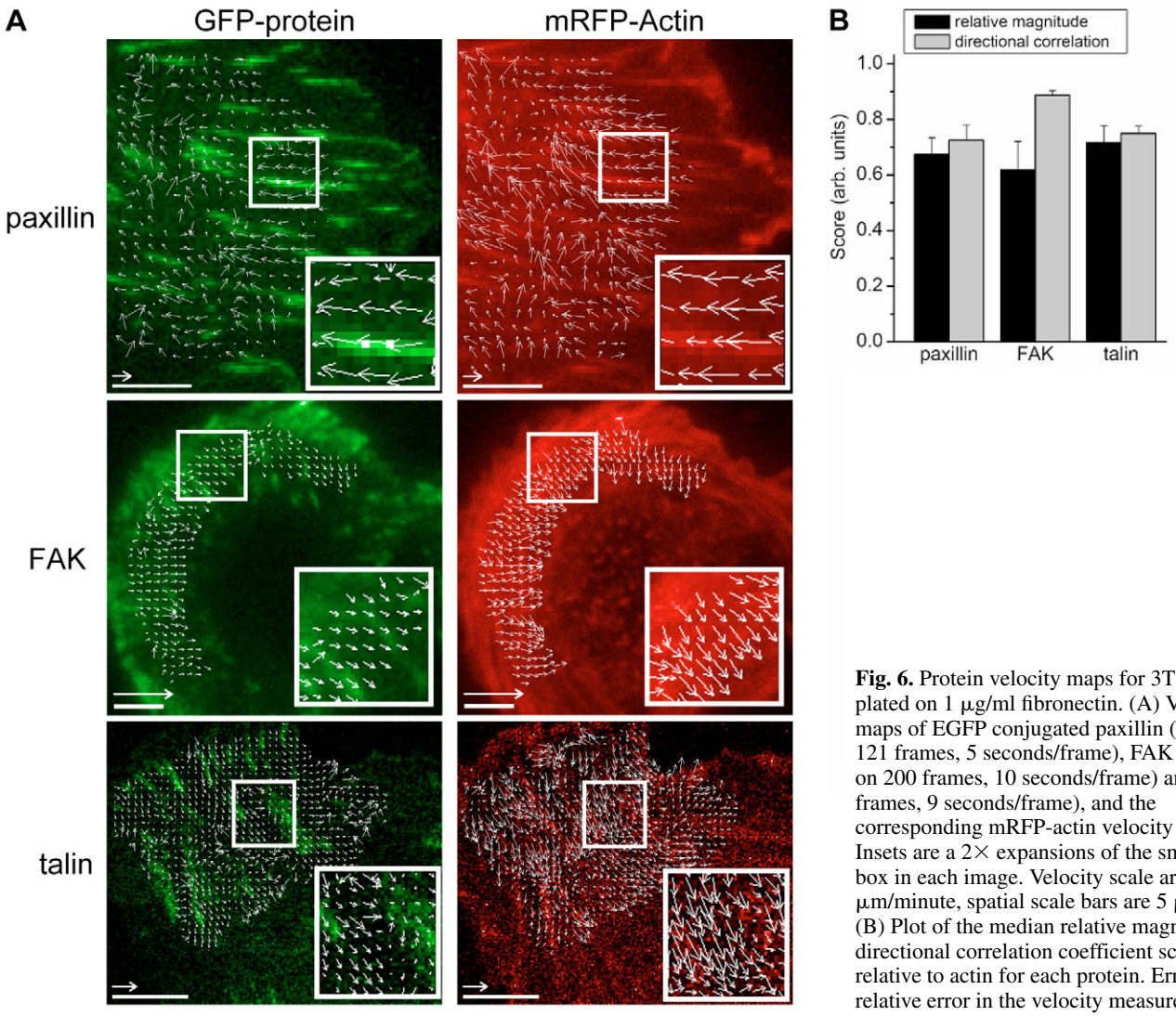

Fig. 6. Protein velocity maps for 3T3 cells plated on 1 μg/ml fibronectin. (A) Velocity maps of EGFP conjugated paxillin (analysis on 121 frames, 5 seconds/frame), FAK (analysis on 200 frames, 10 seconds/frame) and talin (52 frames, 9 seconds/frame), and the corresponding mRFP-actin velocity maps. Insets are a 2× expansions of the small white box in each image. Velocity scale arrows are 1 μm/minute, spatial scale bars are 5 μm. (B) Plot of the median relative magnitude and directional correlation coefficient scores relative to actin for each protein. Error bars are relative error in the velocity measurement.

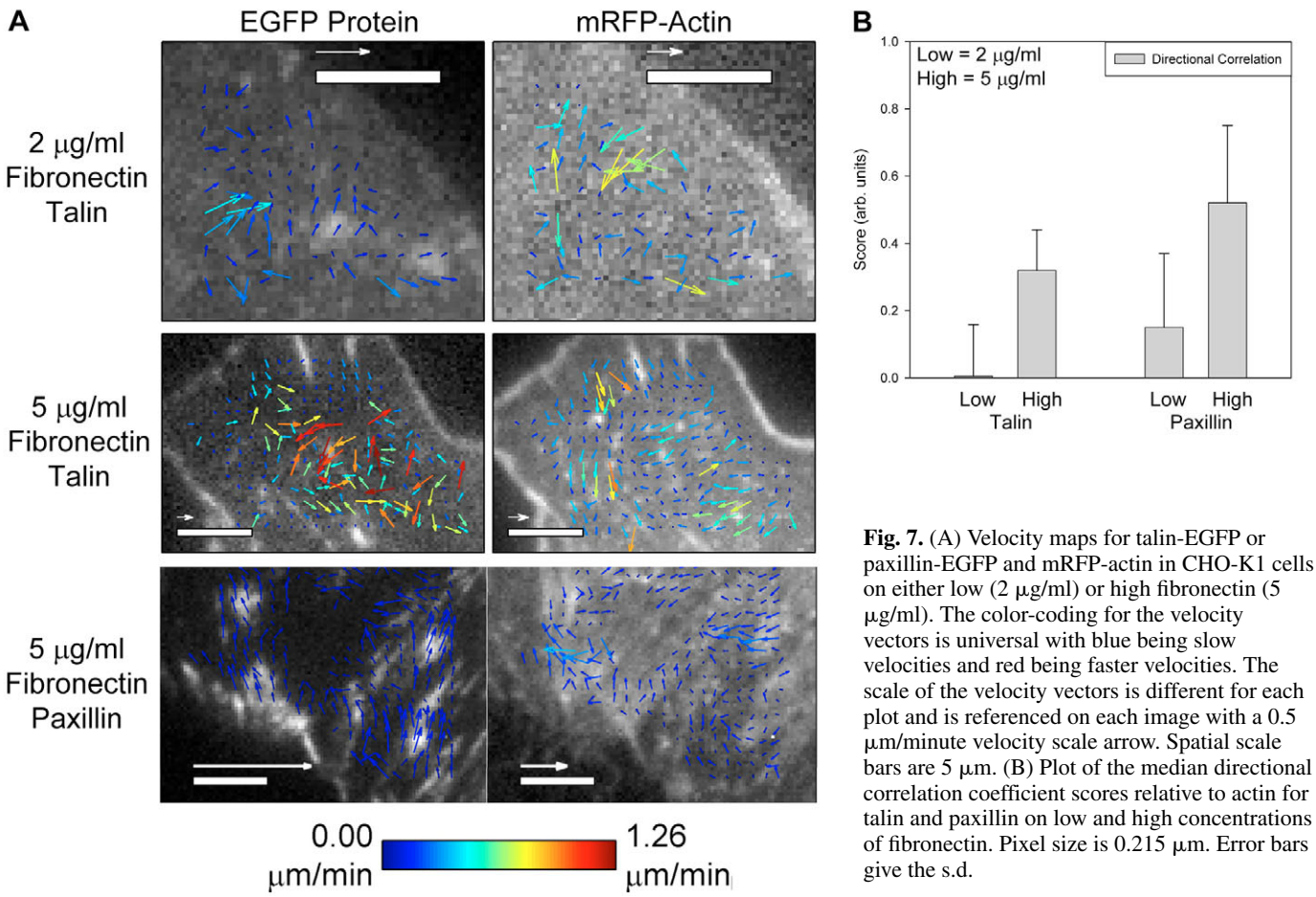

Fig. 7. (A) Velocity maps for talin-EGFP or paxillin-EGFP and mRFP-actin in CHO-K1 cells on either low (2 μg/ml) or high fibronectin (5 μg/ml). The color-coding for the velocity vectors is universal with blue being slow velocities and red being faster velocities. The scale of the velocity vectors is different for each plot and is referenced on each image with a 0.5 μm/minute velocity scale arrow. Spatial scale bars are 5 μm. (B) Plot of the median directional correlation coefficient scores relative to actin for talin and paxillin on low and high concentrations of fibronectin. Pixel size is 0.215 μm. Error bars give the s.d.

linkage appears to be regulated at two levels: through interactions with integrin and with actin (see Fig. 8). On the first level, there are many potential proteins that link integrin to the actin cytoskeleton, however, talin is emerging as a likely candidate (Nayal et al., 2004). Talin is essential for force generation (Jiang et al., 2003), integrin activation (Calderwood et al., 1999) and the stability of junctions (Martel et al., 2001). Although the integrin-talin interaction is relatively weak, it may be highly regulated (Ratnikov et al., 2005) and strong within adhesions. On the second level, there are also several possible candidates that could mediate the connection between the adhesion and actin. α-actinin is a likely candidate because several studies point to α-actinin as a key protein in tension-sensing by adhesions (Laukaitis et al., 2001; von Wichert et al., 2003). The incorporation of α-actinin into adhesions occurs late in their assembly and is coincident with the onset of their retrograde movement (or sliding), suggesting that the adhesions are under higher tension (Laukaitis et al., 2001; Webb et al., 2002). In addition, the force-dependent strengthening of integrin-cytoskeleton linkages correlates with the incorporation of α-actinin into adhesions, and this incorporation is regulated by FAK-dependent phosphorylation on Y12 of α-actinin (Laukaitis et al., 2001; von Wichert et al., 2003). The potential role of α-actinin in tension-sensing and its known binding interactions with both vinculin and talin, which are thought to comprise a structural linkage between integrin and actin (Critchley, 2004; Otto, 1983), make α-actinin a likely candidate for regulation of the ECM-actin linkage via its binding to the one or more adhesion-associated proteins.

This study reveals the power of STICS as a technique that can be used to generate detailed cellular maps of: (1) mobile protein velocities within regions of the cell with high protein densities such as along filamentous structures or within adhesions; (2) mobile protein velocities when protein density and signal contrast are low so that there is no obvious structure to the protein distribution; (3) changes in protein dynamics

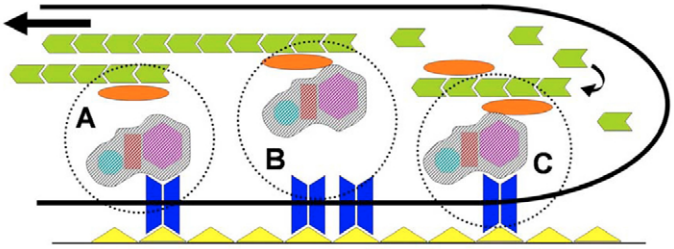

Fig. 8. Model of a protruding lamella illustrating how differential retrograde motion of actin and adhesion proteins can be regulated at two levels in the linkage. The actin (green) and α-actinin (orange) are always concomitant. Slippage occurs either (A) proximal to α-actinin through its interaction with one of the components of the linkage complex (shaded molecules) or (B) proximal to the integrins (blue dimers) perhaps at the talin-integrin linkage. (C) Protrusion can occur through polymerization generated forces when both levels of the adhesion complex are engaged.

following perturbations; (4) regions of the cell where protein dynamics change but are difficult to observe directly, such as the base of the lamella. These analyses are straightforward and can be performed in a matter of minutes on simple time-lapse images collected on virtually any type of fluorescence microscope. Notably, it can be performed on cells that are simply transfected with any type of fluorescently labeled molecule as long as the mobility of the molecules is on the time scale of the imaging rate. The practicality and general applicability of this technique in a wide variety of settings should prove useful in further characterizing the regulation of the ECM-actin linkage and more generally for studying protein movements involved in other diverse cellular phenomena.

Materials and Methods

Tissue culture and treatment

The α-actinin-EGFP, paxillin-EGFP and α5-integrin-EGFP plasmids have been previously described (Laukaitis et al., 2001). The plasmids for β-actin–mRFP and talin-EGFP were generous gifts from the laboratories of Frank Gertler (MIT, Cambridge, MA) and Anna Huttenlocher (University of Wisconsin, Madison, WI), respectively. CHO-K1, 3T3 or MEF cells were cultured in a humidified, 8.5% CO_2 atmosphere at 37°C in minimum essential medium (MEM) supplemented with 10% FBS, non-essential amino acids (for CHO K1 cells) and L-glutamine. Cells were transfected 24-48 hours before experiments, and then imaged by plating in CCM1 medium (Hyclone, UT) buffered with 15 mM HEPES on dishes coated with 1-10 μg/ml fibronectin (Sigma-Aldrich) and maintained at 37°C during imaging with a Warner Instruments heated stage insert (Warner Instruments, Hamden, CT) and a Bioptechs (Bioptechs, Butler, PA) objective heater. Throughout this work, we analysed relatively low expressing cells to avoid artifacts due to overexpression.

Microscopy

TIRF microscopy was performed on an Olympus IX70 microscope equipped with an Olympus TIRF illumination arm and a PlanApo 60× (1.45 NA) oil immersion objective (Olympus, Japan). The laser launch (Prairie Technologies, Inc., Middleton, WI) was connected to the TIRF illumination arm via an optical fiber, and excitation was from a 200 mW argon-ion laser (488 nm, attenuated to ~1% laser power) or a 2 mW helium-neon green laser (543 nm, full power). Images were collected sequentially using MetaMorph software (Molecular Devices Corporation, Downingtown, PA), with AOTF control of the laser lines, and a Retiga EXi camera (QImaging, Burnaby, BC, Canada). Imaging was done using custom dichroic filter sets designed by Chroma Technology Corp. (Rockingham, VT); for EGFP imaging an HQ485/30 dichroic filter was used in combination with a 535/30 bandpass emission filter. For dual EGFP/RFP imaging a z488/543rpc dual dichroic was used in combination with a z488/543 dual band pass emission filter in the cube and a 535/30 or 630/60 emission filter in a LUDL filter wheel to select either EGFP or RFP emission. Confocal images were acquired on an IX70 Olympus Fluoview 300 inverted microscope (Olympus, Japan) as described previously (Wiseman and Brown et al., 2004).

Inhibitor treatments

For inhibitor treatments, a sample of concentrated drug in DMSO was prepared and kept at –20°C. The stock solution was diluted immediately before use in 2 ml of CCM1 imaging medium (Hyclone, UT) heated to 37°C. Cells were imaged for a period of time, then image collection was paused and the medium was removed from the 35-mm tissue culture dish and replaced with 2 ml of medium containing the drug of interest. The 35-mm tissue culture dish remained on the stage of the microscope during the change of media and image collection was resumed immediately with a delay of only 1-2-minutes. Drug concentrations were as follows: 200 nM cytoD, 50 μM blebbistatin, 10 μM Y-27632, 10 μM ML7.

STICS and velocity field analysis

The STICS analysis involves calculating an intensity-fluctuation spatial correlation function over time. The changes in this function directly reflect the underlying transport dynamics of the fluorescently labeled macromolecules in the imaged cell. We define a generalized spatio-temporal intensity-fluctuation correlation function with independent spatial-lag variables ξ and η, and a temporal-lag variable τ for one image-detection channel a:

$$r_{aa}(\xi,\eta,\tau) = \frac{\langle \delta i_a(x,y,t)\, \delta i_a(x+\xi,y+\eta,t+\tau)\rangle}{\langle i_a\rangle_t \langle i_a\rangle_{t+\tau}}, \quad (1)$$

where $\delta i_a(x,y,t) = i_a(x,y,t) - \langle i_a\rangle_t$ is the intensity fluctuation in channel a at image pixel position (x,y) and time t, the angular brackets in the denominator represent spatial ensemble averaging over images at time t and $t+\tau$ in the time series, and the numerator is also an ensemble average over all pixel fluctuations in pairs of images separated by a time-lag of τ.

In practice, we calculate the discrete approximation to the generalized spatio-temporal correlation function as:

$$r_{aa}(\xi,\eta,\tau) = \frac{1}{N-s}\sum_{k=0}^{N-s} \frac{\langle \delta i_a(x,y,k)\, \delta i_a(x+\xi,y+\eta,k+s)\rangle}{\langle i_a\rangle_k \langle i_a\rangle_{k+s}}, \quad (2)$$

where N is the total number of images in the time series, the spatial lag variables ξ and η represent pixel shifts in x and y, and s is the discrete frame-lag between pairs of images in the time series. The real discrete time-lag, $\Delta t \sim \tau$, is simply the product of the frame lag and the sampling time per image frame: $\Delta t = s\delta t$ (where δt is the sampling time per frame). This discrete correlation function is calculated by averaging the spatial cross-correlation of intensity fluctuations between all image pairs separated by the variable time-lag (Δt) in a fluorescence-image time series (see Fig. 1A). The function r_{aa} represents the average cross-correlation function for channel a for all pairs of images separated within the image time series by a lag time of Δt.

If there is concerted translational motion of some of the fluorescent proteins during the imaging, it will be observed in the time evolution of the spatio-temporal correlation function. A directional flow-component peak of the correlation function will start at the center (ξ=0, η=0) at Δt=0 and move away from the center as a function of time lag (see Fig. 1C). The displacement distance and direction of this correlation peak can be tracked giving the underlying flow vector (i.e. magnitude and direction) of the directed protein movement. In the case of random diffusion of the proteins, no directional flow component peak is observed in the correlation function, and the correlation peak stays centered at the origin while it decays in amplitude and spreads out uniformly in space as Δt increases (Fig. 1D) and the proteins diffuse randomly in all directions (Hebert et al., 2005).

The technique is very sensitive because protein motion in regions of the cell where there is visibly diffuse homogenous fluorescence intensity can still be measured, provided that the density of the labeled protein is not too high (<100 μm^{-2}) so as to make the relative intensity fluctuations too small to be measured by the image correlation approach (Costantino et al., 2005).

When the STICS analysis is applied on images with many bright and static structures, the flow-component peak of the correlation function arising from any directed protein movements is 'hidden' within the central persistent correlation peak that arises from the immobile components (see Fig. 1B, arrowhead) and directed movement is not readily detected. An immobile population filtering algorithm was developed for STICS so that the 'hidden' mobile protein components along or near these structures could be detected (Hebert et al., 2005). The algorithm calculates a corrected pixel intensity (i_{new}) by subtracting the average intensity for each pixel time trace from the original pixel intensity (i_{old}). Following the immobile removal the relative intensity fluctuations within a given pixel location are larger. We define the immobile filtered intensity at a single pixel location (p,q) as:

$$i_{new}(p,q,k) = i_{old}(p,q,k) - \frac{1}{N}\sum_{k=0}^{N-1} i_{old}(p,q,k) = i_{old}(p,q,k) - \overline{i(p,q)}, \quad (3)$$

where the summation is over discrete image frames (k) so the subtracted term with the over bar is effectively the time average through the image series of the intensity at image pixel location (p,q).

To demonstrate the effectiveness of the immobile removal algorithm, we analysed a computer simulation with 20% of the population flowing along the x-axis (v_x= –0.1 μm/second, v_y= 0 μm/second) with the remaining 80% of the population immobile. If the immobile component is not filtered using the algorithm, then the translating correlation-function peak owing to flow is 'buried' under the dominant static spatial correlations of the immobile population and is very difficult to detect (Fig. 1A,B, see arrowhead). However, after the filtering algorithm is applied, the static spatial-correlation peak due to immobile components disappears and the flow-component peak can easily be tracked revealing the underlying transport dynamics (compare Fig. 1B and C, see arrowheads). Such motions are not evident from a visual examination of the image time series but can be resolved by the STICS method with immobile filtering even with less than 10% of the labeled protein population actually mobile (data not shown).

Velocity maps were generated by selecting a grid of overlapping, 16×16 pixel square regions (with an overlap of four pixels) that spanned an entire cellular region of interest, and performing the STICS analysis (Hebert et al., 2005) with correction for immobile fraction on each sub-region time stack within this grid. For analyses on cells, these sub-regions were overlapping square areas of approximately 3×3 μm within the images. As a result, regions – both on and off adhesions – were measured within many of the grid regions. However, image series were collected with time intervals in the 5-second to 15-second range; therefore, rapid diffusive movements of cytosolic proteins (on the millisecond time scale) outside of adhesion structures would not be measured. To demonstrate that the measurements in cells with large visible adhesions are dominated by movements within adhesions or along actin filaments, we performed computer simulations generating an image time series

consisting of a system with bright adhesion structures containing 80% immobile particles and 20% mobile particles that moved with a constant velocity (0.1 μm/second) along the adhesion structures. Outside of the adhesions, the particles were a factor of six less bright and 80% of these particles were immobile and 20% were diffusing with a diffusion constant of 1.0 μm^2/second to simulate a rapidly diffusing cytosolic component. STICS analysis with immobile population filtering on these computer simulation image time series detected the directed transport of the 20% population of particles along the adhesions (supplementary material Fig. S1A) and also recovered the set particle velocity of 0.1 μm/second. In regions outside of the adhesion structures no directed motion was detected (supplementary material Fig. S1A). Similar results were found for cellular measurements where analysis of a rectangular region (white rectangle, supplementary material Fig. S1B) or a larger square region encompassing areas around the adhesion (red square, supplementary material Fig. S1B) give similar velocity vectors. Areas outside of adhesions show no measurable velocity (white square, supplementary material Fig. S1B).

To analyse the degree of correlation in the direction of two velocity maps generated for two different detection channels (*a* and *b*), a directional correlation coefficient score was calculated as the cosine of the angle between the two velocity vectors for every point of the map using the dot product formula: $\cos(\theta)=\vec{v}_a\cdot\vec{v}_b/(\|\vec{v}_a\|\times\|\vec{v}_b\|)$. The median of the cosine values is a number that varies between −1 and 1, with the velocity vectors being perfectly anti-aligned at −1, uncorrelated at 0 and perfectly aligned at 1. The error on the median was estimated using the bootstrap method (Efron, 1979). The correlation in velocity magnitude between two vector maps was calculated as the ratio of the magnitudes of the two velocity vectors for every point in the two maps. Throughout the text median values of relative magnitude and direction are presented rather than mean values which are much more sensitive to outliers with large or small correlation coefficients. Analysis was done on a standard desktop PC computer using either Interactive Data Language (IDL 6.0, RSI, Colorado) or MatLab (Natick, MA).

B.H. and D.L.K. were supported by PGS fellowships from the Natural Sciences and Engineering Research Council (NSERC) of Canada and a McGill University Major Fellowship. P.W.W. was supported by grants from NSERC, the Canadian Foundation for Innovation, and the Canadian Institutes of Health Research. A.R.H. and C.M.B. were supported by NIGMS grants GM23244 and U54 GM64346 and the Cell Migration Consortium. Thank you to Jenna Gale for help with data analysis.

References

Axelrod, D. (2001). Total internal reflection fluorescence microscopy in cell biology. *Traffic* **2**, 764-774.

Burridge, K. and Mangeat, P. (1984). An interaction between vinculin and talin. *Nature* **308**, 744-746.

Burridge, K., Nuckolls, G., Otey, C., Pavalko, F., Simon, K. and Turner, C. (1990). Actin-membrane interaction in focal adhesions. *Cell Differ. Dev.* **32**, 337-342.

Calderwood, D. A., Zent, R., Grant, R., Rees, D. J. G., Hynes, R. O. and Ginsberg, M. H. (1999). The talin head domain binds to integrin beta subunit cytoplasmic tails and regulates integrin activation. *J. Biol. Chem.* **274**, 28071-28074.

Costantino, S., Comeau, J. W., Kolin, D. L. and Wiseman, P. W. (2005). Accuracy and dynamic range of spatial image correlation and cross-correlation spectroscopy. *Biophys. J.* **89**, 1251-1260.

Critchley, D. R. (2004). Cytoskeletal proteins talin and vinculin in integrin-mediated adhesion. *Biochem. Soc. Trans.* **32**, 831-836.

Crowley, E. and Horwitz, A. F. (1995). Tyrosine phosphorylation and cytoskeletal tension regulate the release of fibroblast adhesions. *J. Cell Biol.* **131**, 525-537.

Dobereiner, H. G., Dubin-Thaler, B. J., Giannone, G. and Sheetz, M. P. (2005). Force sensing and generation in cell phases: analyses of complex functions. *J. Appl. Physiol.* **98**, 1542-1546.

Efron, B. (1979). Bootstrap methods: another look at the jackknife. *The Annals of Statistics* **7**, 1-26.

Geiger, B. and Bershadsky, A. (2001). Assembly and mechanosensory function of focal contacts. *Curr. Opin. Cell Biol.* **13**, 584-592.

Geiger, B. and Bershadsky, A. (2002). Exploring the neighborhood: adhesion-coupled cell mechanosensors. *Cell* **110**, 139-142.

Geiger, B., Bershadsky, A., Pankov, R. and Yamada, K. M. (2001). Transmembrane extracellular matrix-cytoskeleton crosstalk. *Nat. Rev. Mol. Cell Biol.* **2**, 793-805.

Gupton, S. L. and Waterman-Storer, C. M. (2006). Spatiotemporal feedback between actomyosin and focal-adhesion systems optimizes rapid cell migration. *Cell* **125**, 1361-1374.

Hebert, B., Costantino, S. and Wiseman, P. W. (2005). Spatiotemporal image correlation spectroscopy (STICS) theory, verification, and application to protein velocity mapping in living CHO cells. *Biophys. J.* **88**, 3601-3614.

Horwitz, A., Duggan, K., Buck, C., Beckerle, M. C. and Burridge, K. (1986). Interaction of plasma membrane fibronectin receptor with talin–a transmembrane linkage. *Nature* **320**, 531-533.

Jiang, G., Giannone, G., Critchley, D. R., Fukumoto, E. and Sheetz, M. P. (2003). Two-piconewton slip bond between fibronectin and the cytoskeleton depends on talin. *Nature* **424**, 334-337.

Jurado, C., Haserick, J. R. and Lee, J. (2005). Slipping or gripping? Fluorescent speckle microscopy in fish keratocytes reveals two different mechanisms for generating a retrograde flow of actin. *Mol. Biol. Cell* **16**, 507-518.

Katsumi, A., Naoe, T., Matsushita, T., Kaibuchi, K. and Schwartz, M. A. (2005). Integrin activation and matrix binding mediate cellular responses to mechanical stretch. *J. Biol. Chem.* **280**, 16546-16549.

Lauffenburger, D. A. and Horwitz, A. F. (1996). Cell migration: a physically integrated molecular process. *Cell* **84**, 359-369.

Laukaitis, C. M., Webb, D. J., Donais, K. and Horwitz, A. F. (2001). Differential dynamics of {alpha}5 integrin, paxillin, and {alpha}-actinin during formation and disassembly of adhesions in migrating cells. *J. Cell Biol.* **153**, 1427-1440.

Lin, C.-H. and Forscher, P. (1995). Growth cone advance is inversely proportional to retrograde F-actin flow. *Neuron* **14**, 763-771.

Martel, V., Racaud-Sultan, C., Dupe, S., Marie, C., Paulhe, F., Galmiche, A., Block, M. R. and Albiges-Rizo, C. (2001). Conformation, localization, and integrin binding of talin depend on its interaction with phosphoinositides. *J. Biol. Chem.* **276**, 21217-21227.

Mitchison, T. and Kirschner, M. (1988). Cytoskeletal dynamics and nerve growth. *Neuron* **1**, 761-772.

Nayal, A., Webb, D. J. and Horwitz, A. F. (2004). Talin: an emerging focal point of adhesion dynamics. *Curr. Opin. Cell Biol.* **16**, 94-98.

Otey, C. A., Pavalko, F. M. and Burridge, K. (1990). An interaction between alpha-actinin and the beta 1 integrin subunit in vitro. *J. Cell Biol.* **111**, 721-729.

Otto, J. J. (1983). Detection of vinculin-binding proteins with an 125I-vinculin gel overlay technique. *J. Cell Biol.* **97**, 1283-1287.

Palecek, S. P., Schmidt, C. E., Lauffenburger, D. A. and Horwitz, A. F. (1996). Integrin dynamics on the tail region of migrating fibroblasts. *J. Cell Sci.* **109**, 941-952.

Palecek, S. P., Huttenlocher, A., Horwitz, A. F. and Lauffenburger, D. A. (1998). Physical and biochemical regulation of integrin release during rear detachment of migrating cells. *J. Cell Sci.* **111**, 929-940.

Pavalko, F. M. and Burridge, K. (1991). Disruption of the actin cytoskeleton after microinjection of proteolytic fragments of alpha-actinin. *J. Cell Biol.* **114**, 481-491.

Peskin, C. S., Odell, G. M. and Oster, G. F. (1993). Cellular motions and thermal fluctuations: the Brownian ratchet. *Biophys. J.* **65**, 316-324.

Ponti, A., Machacek, M., Gupton, S. L., Waterman-Storer, C. M. and Danuser, G. (2004). Two distinct actin networks drive the protrusion of migrating cells. *Science* **305**, 1782-1786.

Ratnikov, B., Ptak, C., Han, J., Shabanowitz, J., Hunt, D. F. and Ginsberg, M. H. (2005). Talin phosphorylation sites mapped by mass spectrometry. *J. Cell Sci.* **118**, 4921-4923.

Regen, C. M. and Horwitz, A. F. (1992). Dynamics of beta 1 integrin-mediated adhesive contacts in motile fibroblasts. *J. Cell Biol.* **119**, 1347-1359.

Ridley, A. J., Schwartz, M. A., Burridge, K., Firtel, R. A., Ginsberg, M. H., Borisy, G., Parsons, J. T. and Horwitz, A. R. (2003). Cell migration: integrating signals from front to back. *Science* **302**, 1704-1709.

Sampath, P. and Pollard, T. D. (1991). Effects of cytochalasin, phalloidin and pH on the elongation of actin filaments. *Biochemistry* **30**, 1973-1980.

Sato, M., Schwarz, W. H. and Pollard, T. D. (1987). Dependence of the mechanical properties of actin/alpha-actinin gels on deformation rate. *Nature* **325**, 828-830.

Smilenov, L. B., Mikhailov, A., Pelham, R. J., Jr, Marcantonio, E. E. and Gundersen, G. G. (1999). Focal adhesion motility revealed in stationary fibroblasts. *Science* **286**, 1172-1174.

Straight, A. F., Cheung, A., Limouze, J., Chen, I., Westwood, N. J., Sellers, J. R. and Mitchison, T. J. (2003). Dissecting temporal and spatial control of cytokinesis with a myosin II inhibitor. *Science* **299**, 1743-1747.

Sydor, A. M., Su, A. L., Wang, F. S., Xu, A. and Jay, D. G. (1996). Talin and vinculin play distinct roles in filopodial motility in the neuronal growth cone. *J. Cell Biol.* **134**, 1197-1207.

Vallotton, P., Ponti, A., Waterman-Storer, C. M., Salmon, E. D. and Danuser, G. (2003). Recovery, visualization, and analysis of actin and tubulin polymer flow in live cells: A fluorescent speckle microscopy study. *Biophys. J.* **85**, 1289-1306.

Vallotton, P., Danuser, G., Bohnet, S., Meister, J. and Verkhovsky, A. B. (2005). Tracking retrograde flow in keratocytes: news from the front. *Mol. Biol. Cell* **16**, 1223-1231.

Vicente-Manzanares, M., Webb, D. J. and Horwitz, A. R. (2005). Cell migration at a glance. *J. Cell Sci.* **118**, 4917-4919.

von Wichert, G., Haimovich, B., Feng, G.-S. and Sheetz, M. P. (2003). Force-dependent integrin-cytoskeleton linkage formation requires downregulation of focal complex dynamics by Shp2. *EMBO J.* **22**, 5023-5035.

Waterman-Storer, C. M., Desai, A., Chloe Bulinski, J. and Salmon, E. D. (1998). Fluorescent speckle microscopy, a method to visualize the dynamics of protein assemblies in living cells. *Curr. Biol.* **8**, 1227-1230.

Webb, D. J., Donais, K., Whitmore, L. A., Thomas, S. M., Turner, C. E., Parsons, J. T. and Horwitz, A. F. (2004). FAK-Src signalling through paxillin, ERK and MLCK regulates adhesion disassembly. *Nat. Cell. Biol.* **6**, 154-161.

Webb, D. J., Parsons, J. T. and Horwitz, A. F. (2002). Adhesion assembly, disassembly and turnover in migrating cells – over and over and over again. *Nat. Cell Biol.* **4**, E97-E100.

Wiseman, P. W., Brown, C. M., Webb, D. J., Hebert, B., Johnson, N. L., Squier, J. A., Ellisman, M. H. and Horwitz, A. F. (2004). Spatial mapping of integrin interactions and dynamics during cell migration by Image Correlation Microscopy. *J. Cell Sci.* **117**, 5521-5534.